AIAA Guidance, Navigation, and Control Conference and Exhibit
21 - 24 August 2006, Keystone, Colorado

AIAA 2006-6716

Adaptive, Integrated Guidance and Control Design for Line-of-Sight based Formation Flight

Byoung Soo Kim*
Gyeongsang National University, Gyeongnam, SOUTH KOREA

Anthony J. Calise† and Ramachandra J. Sattigeri‡
Georgia Institute of Technology, Atlanta, GA 30332-0150

This paper presents an integrated guidance and control design for formation flight using a combination of adaptive output feedback and backstepping techniques without an underlying time-scale separation assumption. We formulate the problem as an adaptive output feedback control problem for a line-of-sight (LOS) based formation flight configuration of a leader and a follower aircraft. The design objective is to regulate range and two bearing angle rates while maintaining turn coordination. Adaptive neural networks are trained online with available measurements to compensate for unmodeled nonlinearities in the design process. These include uncertainties due to unknown leader aircraft acceleration, and the modeling error due to parametric uncertainties in the aircraft aerodynamic derivatives. One benefit of this approach is that the guidance and flight control design process is integrated. Simulation results using a nonlinear 6DOF simulation model are presented to illustrate the efficacy of the approach by comparing the performance with a time-scale separation based design.

I. Introduction

AS demonstrated in recent conflicts, unmanned aerial vehicles (UAVs) are becoming an important component of our military force structure. UAVs, operating in close proximity to enemy forces, provide real-time information difficult to obtain from other sources, without risk to human pilots. Among the strategies employed by these UAVs will be flocks of cooperative MAVs operating in close proximity to terrain or structures that will gather information and, under human supervision, seek out, identify, and engage targets. They will be expected to maintain a formation while at the same time executing searches in a congested environment. Stealth like operations will also be important, implying the need to maintain autonomy and to minimize communication. Maintaining a formation is also important from this perspective so that passive sensing can be used to ascertain the locations and behaviors of cooperating MAVs/UAVs.

The problem of leader-follower formation flight in which the follower aircraft is equipped with only an onboard camera to track the leader aircraft is quite challenging. This problem requires simultaneous sensor data processing, state estimation and tracking control in the presence of unmodeled disturbances (leader acceleration) and measurement uncertainties. Sensor data processing involves fast converging image processing algorithms that track the leader aircraft in the presence of background clutter and derive noisy measurements of the leader aircraft's position relative to itself [1,2]. A consequence of using a monocular fixed camera is that the range becomes unobservable. So the measurements from the image processing algorithm are fed into a nonlinear filter, e.g., an Extended Kalman Filter (EKF), which computes estimates of range and other line-of-sight (LOS) variables that are required in the guidance and control algorithms [1]. Assuming that we have useful estimates of the range and other required LOS variables, regulating these variables to desired values is not an easy problem. In Ref. 3, an adaptive guidance algorithm and an adaptive autopilot were designed separately using time-scale separation argument, and then integrated together to enable the follower aircraft to maintain close range (about two wing-span lengths) from a maneuvering leader aircraft. True values of range and LOS azimuth and elevation angles were assumed, i.e., the

* Associate Professor, School of Mechanical and Aerospace Engineering, bskim@gsnu.ac.kr, AIAA Member. Visiting Scholar at Georgia Tech.
† Professor, School of Aerospace Engineering, anthony.calise@ae.gatech.edu, Fellow AIAA.
‡ Graduate Research Assistant, School of Aerospace Engineering, gte334x@prism.gatech.edu, AIAA Member.

Copyright © 2006 by Byoung Soo Kim and Anthony J. Calise. Published by the American Institute of Aeronautics and Astronautics, Inc., with permission.

image processing and nonlinear state filters were not implemented. Even in this case, it was found that the leader acceleration has a degrading effect on the range tracking performance. It was observed that when the leader maneuver was severe, for example a sharp heading change, the guidance algorithm of the follower would send large commands to the autopilot and cause the actuators to saturate. Consequently, the guidance commands to the autopilot were scaled down by a fixed factor to ensure closed-loop stability for a range of leader aircraft maneuvers [3]. This scaling factor was arrived at after several simulation runs. The scaling down of the guidance commands resulted in larger overshoots from the commanded range as the severity of the leader maneuver increased. Hence performance was compromised to ensure stability.

Conventional approaches to guidance and flight control design employ a time-scale separation argument to justify the separate design of the guidance and autopilot subsystems. Once designed, the two subsystems are integrated together and tuned till the performance objectives are satisfied. While this approach to design has been successfully implemented on many flight vehicle systems, the design usually results in an overall performance that is less than what can be achieved. This is because the conventional approach ignores the coupling between the guidance and autopilot subsystems. Secondly, in high performance applications like intercepting a highly maneuvering target, or maintaining range from a maneuvering leader aircraft in a formation, the time-scale separation argument does not hold. In such cases the guidance subsystem can drive the autopilot and the overall system unstable with commands that cannot be achieved by the autopilot. Integrated approaches to guidance and control design have been indicated in literature as a way to overcome the shortcomings of the conventional approach. Its been stated that an integrated guidance and control (IGC) formulation can directly compensate for the effect of autopilot lag and improve missile intercept performance [4,5]. An integrated approach also helps avoid the iterative procedure involved in tuning the guidance and autopilot subsystems, if designed separately. The integrated design is also less susceptible to saturation and stability problems. Feedback linearization of the relative cross-range and altitude to target and the roll-angle is employed in Refs. 4-5 for the IGC formulation. Sliding mode control theory is employed in Ref. 6 for the IGC formulation. In Ref. 7, a single-plane linear IGC problem formulation is considered and a game-theoretic control synthesis approach is utilized. In Ref. 8, the IGC problem is formulated as a finite-time horizon nonlinear disturbance attenuation problem. An approximate solution approach to the above problem is developed that is referred to as the state-dependent Riccati differential (difference) equation (SDRDE) technique. Monte Carlo simulation results using this technique showed that it performed favorably compared to a benchmark guidance and control system and resulted in much smaller overall system time constants. The SDRDE technique however is computationally intensive owing to the need to solve Riccati difference equations online at each sample instant. An adaptive backstepping based approach to IGC design is presented in Ref. 9. The missile dynamics have to be written in the strict-feedback form [10] in order to use the backstepping approach. The advantage is that the backstepping approach can directly address plants with unmatched uncertainties. Adaptation is included to provide robustness to parametric uncertainty in the missile dynamics. In Ref. 11, the flight control system design is done via a conventional inner and outer-loop design approach. The linear compensator gains in the inner and outer-loops are chosen such that the combined error dynamics of both the loops are asymptotically stable in the absence of modeling uncertainties, and thus mitigate inner and outer-loop interaction. Adaptation is included in both loops to address any modeling uncertainties. Pseudo-Control Hedging [12] is used in the inner-loop to prevent adaptation to actuator saturation and dynamics. Hedging is also used in the outer-loop to prevent adaptation to inner-loop dynamics.

The contribution of this paper lies in presenting an adaptive approach to IGC design for a LOS based formation flight configuration of a leader and a follower aircraft. The design objective is to regulate range and two bearing angle rates to specified values while maintaining turn coordination. The bearing angles are defined to be the angles between the LOS vector to the leader aircraft and the optical axis of the camera, which is assumed to be fixed to the body-frame of the follower aircraft. We assume that estimates of these LOS variables are available from the use of on board vision sensors and nonlinear filtering algorithms [1,17]. These LOS variables are differentiated until the actuator deflection terms appear. We show the existence of a well-defined vector relative degree [15] for the MIMO system of the LOS variables with respect to the actuator deflections. Then we perform approximate dynamic inversion of the LOS variable dynamics. Adaptive neural networks are trained online with available measurements to compensate for unmodeled nonlinearities in the design process. These include uncertainties due to unknown leader aircraft acceleration, and the modeling error due to parametric uncertainties in the aircraft aerodynamic derivatives. However, in order to improve turn coordination performance and efficiency in controlling the azimuth bearing angle rate, the design of the LOS azimuth channel is modified using an adaptive backstepping algorithm. One benefit of this approach is that the guidance and flight control design process is integrated. Furthermore, on-line adaptation imbues the integrated system with robustness to the unmodeled nonlinearities. This has a secondary benefit of streamlining the design approach. Simulation results using a nonlinear 6DOF simulation model are presented to illustrate the efficacy of the approach by comparing the performance with a time-scale separation based

design.

The organization of the paper is as follows. Section II provides general information about LOS-based formation flight for UAVs. Section III derives the LOS variable dynamics and shows existence of well-defined vector relative degree for this problem. The control design formulation is described in detail with a summary of the relevant theory. The control design presented in this section is referred to as IGC Design 1. In Section IV, the control designs for the azimuth channel and for maintaining turn coordination are modified to compensate for a drawback in IGC Design 1 that causes unacceptably large sideslip angles during turning maneuvers. The modified design in this section is referred to as IGC Design 2. In Section V the results of simulation and their discussion are given. Section VI presents the conclusions.

II. LOS-based Formation Flight for UAVs

The objective of the formation flight experiment will be for the follower aircraft to maintain a prescribed relative position from the leader aircraft in the presence of leader maneuvers and other unmodeled disturbances. No communication between the UAVs is assumed. The follower UAV is equipped with just one fixed camera for passive sensing of the LOS information. The complete closed-loop system is summarized in the block diagram in Fig. 1.

The Image Processing and Computer Vision block takes as input the image frames from the onboard camera and processes them in real-time for visual tracking of a target (leader) aircraft. This block utilizes the method of *geometric active contours* [1,16] to track various features of interest in the image frames over a period of time. Active contours have the ability to conform to various object shapes and motions, making them ideal for segmentation, edge detection, shape modeling and visual tracking. Level set methods allow for fast, robust implementations of the active contours algorithms [1,16].

For the purposes of formation flight, the IGC block needs estimates of range and LOS angles between the leader and follower to compute commands to the control effectors of the follower. While the LOS angles are available from the images, the range is not. To estimate range from angle measurements, various implementations of an EKF are possible [1,17], and could be augmented with an adaptive element for robust estimation in the presence of unmodeled dynamics and disturbances [18]. At this stage we have not integrated the image processing and estimation to our integrated guidance and control algorithm. Presently, we are using the true values of the range and LOS angles. An approximate differentiator operates on LOS angles to provide estimates of LOS angle rates [3].

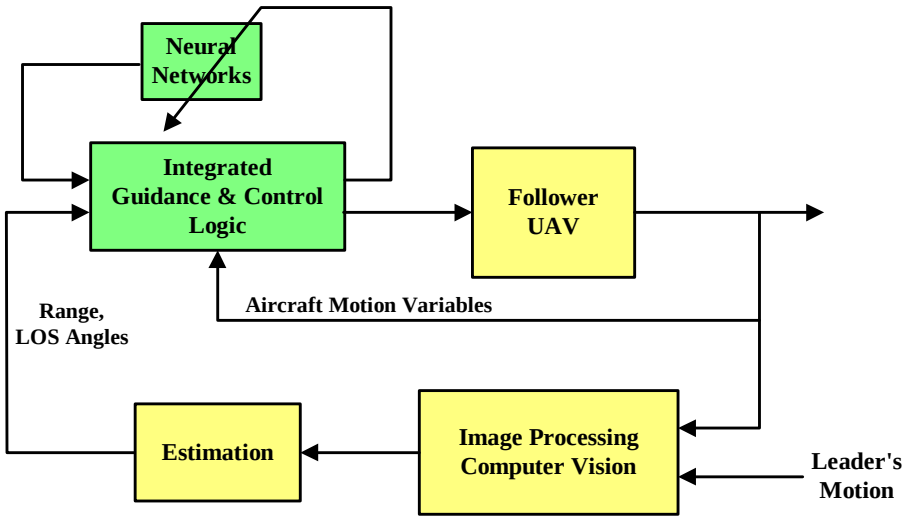

Figure 1. Closed-loop UAV System for LOS-based Formation Flight

III. Integrated Guidance and Control using Neural Networks – Design 1

This section presents an adaptive approach to IGC design for LOS based formation flight. We formulate the problem as an adaptive output feedback control problem for a leader-follower formation flight configuration.

A. Line-of-Sight (LOS) Variable Dynamics

The spherical coordinates consist of the range (R) to the leader, azimuth angle (λ_A) from the inertial X-axis to the projection of the LOS vector onto the X-Y plane, and elevation angle (λ_E) to the horizontal (inertial X-Y plane). These variables are given in terms of the components of the LOS vector in the inertial frame in Fig. 2, which is basically an Earth-surface fixed frame.

$$R = \sqrt{R_X^2 + R_Y^2 + R_Z^2} \tag{1}$$

$$\lambda_A = \tan^{-1}\left(\frac{R_Y}{R_X}\right) \tag{2}$$

$$\lambda_E = \tan^{-1}\left(\frac{-R_Z}{\sqrt{R_X^2 + R_Y^2}}\right) \tag{3}$$

The inertial frame components of the LOS vector are given in terms of the spherical coordinates as

$$R_X = R\cos\lambda_A \cos\lambda_E \tag{4}$$

$$R_Y = R\sin\lambda_A \cos\lambda_E \tag{5}$$

$$R_Z = -R\sin\lambda_E \tag{6}$$

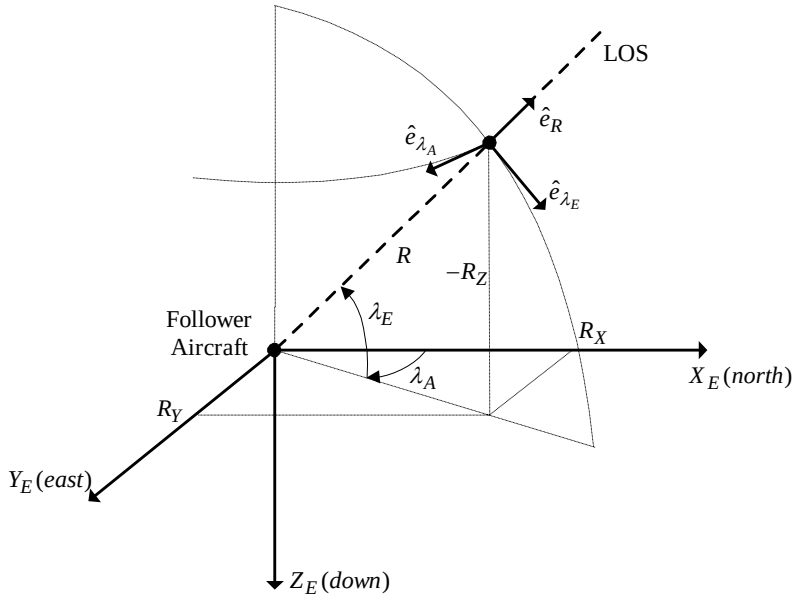

Figure 2. Inertial Coordinate and Spherical Coordinate of Line-of-Sight (LOS)

By differentiating Eq.(1) with respect to time and utilizing Eq.(4)-(6), we can obtain the range dynamics

$$\dot{R} = \dot{R}_X \cos\lambda_A \cos\lambda_E + \dot{R}_Y \sin\lambda_A \cos\lambda_E - \dot{R}_Z \sin\lambda_E \tag{7}$$

After taking tangent on both sides of Eq.(2) and (3), we can obtain the LOS angle dynamics by differentiating and utilizing Eq.(3)-(6)

$$\dot{\lambda}_A = \frac{1}{R\cos\lambda_E}\left(-\dot{R}_X \sin\lambda_A + \dot{R}_Y \cos\lambda_A\right) \tag{8}$$

$$\dot{\lambda}_E = -\frac{1}{R}\left(\dot{R}_X \cos\lambda_A \sin\lambda_E + \dot{R}_Y \sin\lambda_A \sin\lambda_E + \dot{R}_Z \cos\lambda_E\right) \tag{9}$$

where $\dot{R}_X, \dot{R}_Y, \dot{R}_Y$ denote the relative velocity components between the leader and follower aircraft expressed in the inertial coordinate system, which are related to range rate and LOS rate as follows:

$$\dot{R}_X = \dot{R}\cos\lambda_A \cos\lambda_E - R\dot{\lambda}_A \sin\lambda_A \cos\lambda_E - R\dot{\lambda}_E \cos\lambda_A \sin\lambda_E \tag{10}$$

$$\dot{R}_Y = \dot{R}\sin\lambda_A \cos\lambda_E + R\dot{\lambda}_A \cos\lambda_A \cos\lambda_E - R\dot{\lambda}_E \sin\lambda_A \sin\lambda_E \tag{11}$$

$$\dot{R}_Z = -\dot{R}\sin\lambda_E - R\dot{\lambda}_E \cos\lambda_E \tag{12}$$

By differentiating Eq.(7)-(9) and utilizing Eq.(10)-(12), we obtain the following relation between the relative accelerations and the second time derivatives of the range and LOS angles:

$$\ddot{R} = R\left[\dot{\lambda}_A^2 \cos^2\lambda_A + \dot{\lambda}_E^2\right] + \left[a_{X_I} \cos\lambda_A \cos\lambda_E + a_{Y_I} \sin\lambda_A \cos\lambda_E - a_{Z_I} \sin\lambda_E\right] \tag{13}$$

$$\ddot{\lambda}_A = \frac{1}{\cos\lambda_E}\left\{-2\dot{\lambda}_A\left[\left(\frac{\dot{R}}{R}\right)\cos\lambda_E - \dot{\lambda}_E \sin\lambda_E\right] + \left(\frac{1}{R}\right)\left[-a_{X_I} \sin\lambda_A + a_{Y_I} \cos\lambda_A\right]\right\} \tag{14}$$

$$\ddot{\lambda}_E = -2\left(\frac{\dot{R}}{R}\right)\dot{\lambda}_E - \dot{\lambda}_A^2 \sin\lambda_E \cos\lambda_E - \left(\frac{1}{R}\right)\left[a_{X_I} \cos\lambda_A \sin\lambda_E + a_{Y_I} \sin\lambda_A \sin\lambda_E + a_{Z_I} \cos\lambda_E\right] \tag{15}$$

where $a_{X_I} = a_{L_{X_I}} - a_{F_{X_I}} \equiv \ddot{R}_X$, $a_{Y_I} = a_{L_{Y_I}} - a_{F_{Y_I}} \equiv \ddot{R}_Y$, $a_{Z_I} = a_{L_{Z_I}} - a_{F_{Z_I}} \equiv \ddot{R}_Z$ are the relative accelerations of the leader with respect to the follower in the inertial plane. Subscripts '*L*' and '*F*' denote leader and follower aircraft, respectively.

B. Control Formulation

The standard form of the equations of motion used for describing formation flight can be written as

$$\dot{\bar{x}} = f(\bar{x}, \bar{a}_L) + \sum_{i=1}^{4} g_i(\bar{x}) u_i \quad \text{and} \quad \bar{y} = h(\bar{x}) \tag{16}$$

where state vector : $\bar{x} = \left[\, U \;\; V \;\; W \;\; p \;\; q \;\; r \;\; \Phi \;\; \Theta \;\; \Psi \;\; R \;\; \lambda_A \;\; \lambda_E \;\; \dot{R} \;\; \dot{\lambda}_A \;\; \dot{\lambda}_E \,\right]^T$,

input vector : $\bar{u} = \left[\, \delta T \;\; \delta a \;\; \delta e \;\; \delta r \,\right]^T$, $\bar{u}(t) \in R^4$

output vector : $\bar{y} = \left[R,\ \dot{\lambda}_A - \dot{\Psi},\ \dot{\lambda}_E - \dot{\Theta},\ \Phi\right]^T$, $\bar{y}(t) \in R^4$

leader motion state vector: $\bar{a}_L = \left[a_{L_{X_I}}, a_{L_{Y_I}}, a_{L_{Z_I}}\right]^T$

The vector $\left[U\ V\ W\right]^T$ is the translational velocity along the body-fixed axes, $\left[p\ q\ r\right]^T$ is the angular velocity vector, $\left[\Phi\ \Theta\ \Psi\right]^T$ is the vector of Euler attitude angles, and the vector $\bar{a}_L$ consists of the leader acceleration terms. Eq.(16) is composed of the conventional 6 DOF aircraft dynamics and the LOS dynamics in Eq.(7)-(9) where $\left\{\delta T\ \delta a\ \delta e\ \delta r\right\}$ represent throttle, aileron, elevator, and rudder deflections as control variables, respectively.

The objective of the control law design is for the follower aircraft to maintain a prescribed range to the leader aircraft in the presence of leader maneuvers and other unmodeled disturbances. In the formulation, the output variables to be regulated are chosen as $\left[R,\ \dot{\lambda}_A - \dot{\Psi},\ \dot{\lambda}_E - \dot{\Theta},\ \Phi\right]^T$. The bank angle Φ command is constructed to maintain turn coordination, that is, to nullify the side acceleration along the Y-axis of the body fixed frame. The range command is given by a constant value, which is chosen as the length of two wing spans in the examples that follow. The variables $\chi_A \equiv \lambda_A - \Psi$ and $\chi_E \equiv \lambda_E - \Theta$ represent the bearing angles in the camera image plane. The bearing angle rate commands are set to zero. The bearing angles are not regulated since it is not desirable to restrict the follower aircraft to a particular orientation with respect to the leader aircraft, particularly in the presence of leader maneuvers.

1. Relative Degree and Approximate Feedback Linearization

To show the existence of a well-defined vector relative degree, the output variables are differentiated until the control variables appear. The first step in this direction is to transform the follower acceleration terms $\left\{a_{F_{X_I}}, a_{F_{Y_I}}, a_{F_{Z_I}}\right\}$, in Eq.(13)-(15) in the inertial frame, into the follower body-axes coordinate frame. It is also preferred to use the specific force vector in the body-axes coordinate frame instead of the acceleration vector, since the specific force vector is a directly measured quantity. This is accomplished by first subtracting the gravity vector,

$$\begin{bmatrix} a_{F_{X_B}} \\ a_{F_{Y_B}} \\ a_{F_{Z_B}} \end{bmatrix} = L_x(\Phi)L_y(\Theta)L_z(\Psi) \cdot \left(\begin{bmatrix} a_{F_{X_I}} \\ a_{F_{Y_I}} \\ a_{F_{Z_I}} \end{bmatrix} - \begin{bmatrix} 0 \\ 0 \\ g \end{bmatrix} \right) \tag{17}$$

which implies,

$$\begin{bmatrix} a_{F_{X_I}} \\ a_{F_{Y_I}} \\ a_{F_{Z_I}} \end{bmatrix} = L_z(-\Psi)L_y(-\Theta)L_x(-\Phi) \begin{bmatrix} a_{F_{X_B}} \\ a_{F_{Y_B}} \\ a_{F_{Z_B}} \end{bmatrix} + \begin{bmatrix} 0 \\ 0 \\ g \end{bmatrix} \tag{18}$$

In Eq. (17), (18) the variable L represents a rotation matrix and the subscript indicates the axis about which the rotation occurs. The terms $\{a_{F_{X_B}}, a_{F_{Y_B}}, a_{F_{Z_B}}\}$ are measurable acceleration components in the body fixed coordinates and will be used in feedback loop in the controller. It is assumed that only the X-component of $\{a_{F_{X_B}}, a_{F_{Y_B}}, a_{F_{Z_B}}\}$ has a functional relation to the throttle among the control input variables $\{\delta T, \delta a, \delta e, \delta r\}$ of the follower aircraft. The Y- and Z-components are assumed to be independent of the control input variables since their dependency is secondary. Thus

$$a_{F_{X_B}} = a_{F_{X_{B_0}}} + \Delta a_{F_{X_B}} \tag{19}$$

where $a_{F_{X_{B0}}} = \left(\Im_{A_{X_0}} + \Im_{T_{X_0}}\right)/m$, $\Delta a_{F_{X_B}} = \left(\Delta\Im_{A_X} + \Delta\Im_{T_X}\right)/m = \cdots + X_{\delta T}\cdot\delta T$, where $\Im$ refers to the external force acting on the aircraft, and the variables $\Im_A, \Im_T$ refer to the external force due to aerodynamics and thrust respectively. Combining Eq.(18) and (19) into Eq.(13)-(15), we obtain

$$\begin{bmatrix} \ddot{R} \\ \ddot{\lambda}_A \\ \ddot{\lambda}_E \end{bmatrix} = \begin{bmatrix} \overline{\Delta}_R \\ \overline{\Delta}_{\lambda_A} \\ \overline{\Delta}_{\lambda_E} \end{bmatrix} + \begin{bmatrix} -\cos(\Psi-\lambda_A)\cos\lambda_E\cos\Theta - \sin\lambda_E\sin\Theta \\ -\sin(\Psi-\lambda_A)\cos\Theta/R\cos\lambda_E \\ \left\{\cos(\Psi-\lambda_A)\sin\lambda_E\cos\Theta - \cos\lambda_E\sin\Theta\right\}/R \end{bmatrix}\cdot X_{\delta T}\,\delta T \tag{20}$$

where the vector $\left[\overline{\Delta}_R, \overline{\Delta}_{\lambda_A}, \overline{\Delta}_{\lambda_E}\right]^T$ is a function of the LOS variables, the leader acceleration terms, and the follower aircraft motion variables.

The next step is to obtain the time derivatives of the Euler angles Ψ, Θ and Φ in terms of the remaining control effectors. To do this, first consider the relationship between the Euler angle rates and the angular velocities [21],

$$\begin{aligned} \dot{\Phi} &= p + \left(q\sin\Phi + r\cos\Phi\right)\tan\Theta \\ \dot{\Theta} &= q\cos\Phi - r\sin\Phi \\ \dot{\Psi} &= \left(q\sin\Phi + r\cos\Phi\right)\sec\Theta \end{aligned} \tag{21}$$

and thus the second time derivatives of Euler angles $\{\Phi,\ \Theta,\ \Psi\}$ can be expressed in the form:

$$\begin{aligned} \ddot{\Phi} &= \dot{p} + \left(\dot{q}\sin\Phi + \dot{r}\cos\Phi\right)\tan\Theta \ +\ \Delta_\Phi \\ \ddot{\Theta} &= \dot{q}\cos\Phi - \dot{r}\sin\Phi \ +\ \Delta_\Theta \\ \ddot{\Psi} &= \left(\dot{q}\sin\Phi + \dot{r}\cos\Phi\right)\sec\Theta \ +\ \Delta_\Psi \end{aligned} \tag{22}$$

where $\{\Delta_\Phi, \Delta_\Theta,\ \Delta_\Psi\}$ are functions of the angular velocities and Euler angles. The derivatives of the angular velocities $\{\dot{p},\ \dot{q},\ \dot{r}\}$ depend mainly on the control surface perturbations $\{\delta a, \delta e, \delta r\}$,

$$\begin{aligned} \dot{p} &= \Delta_p(\bar{x}) \ +\ L_{\delta a}\cdot\delta a \\ \dot{q} &= \Delta_q(\bar{x}) \ +\ M_{\delta e}\cdot\delta e \\ \dot{r} &= \Delta_r(\bar{x}) \ +\ N_{\delta r}\cdot\delta r \end{aligned} \tag{23}$$

where $\{\Delta_p, \Delta_q,\ \Delta_r\}$ are functions of the states of the aircraft dynamics. Using Eq.(23) in Eq.(22), we obtain:

$$\begin{aligned} \ddot{\Phi} &= \Delta'_\Phi(\bar{x}) + L_{\delta a}\cdot\delta a + M_{\delta e}\sin\Phi\tan\Theta\cdot\delta e + N_{\delta r}\cos\Phi\tan\Theta\cdot\delta r \\ \ddot{\Theta} &= \Delta'_\Theta(\bar{x}) + M_{\delta e}\cos\Phi\cdot\delta e - N_{\delta r}\sin\Phi\cdot\delta r \\ \ddot{\Psi} &= \Delta'_\Psi(\bar{x}) + M_{\delta e}\sin\Phi\sec\Theta\cdot\delta e + N_{\delta r}\cos\Phi\sec\Theta\cdot\delta r \end{aligned} \tag{24}$$

Thus, we have the following relations

$$\begin{bmatrix} \ddot{R} \\ \ddot{\lambda}_A - \ddot{\Psi} \\ \ddot{\lambda}_E - \ddot{\Theta} \\ \ddot{\Phi} \end{bmatrix} = \begin{bmatrix} \\ \overline{\Delta}(\bar{x}, \bar{a}_L, t) \\ \\ \end{bmatrix} + \begin{bmatrix} \\ A(\bar{x}) \\ \\ \end{bmatrix} \begin{bmatrix} \delta T \\ \delta a \\ \delta e \\ \delta r \end{bmatrix} \tag{25}$$

where

$$A(\bar{x}) = \begin{bmatrix} -X_{\delta T}\{\cos(\Psi-\lambda_A)\cos\lambda_E\cos\Theta+\sin\lambda_E\sin\Theta\} & 0 & 0 & 0 \\ -X_{\delta T}\sin(\Psi-\lambda_A)\cos\Theta/R\cos\lambda_E & 0 & -M_{\delta e}\sin\Phi\sec\Theta & -N_{\delta r}\cos\Phi\sec\Theta \\ X_{\delta T}\{\cos(\Psi-\lambda_A)\sin\lambda_E\cos\Theta-\cos\lambda_E\sin\Theta\}/R & 0 & -M_{\delta e}\cos\Phi & N_{\delta r}\sin\Phi \\ 0 & L_{\delta a} & M_{\delta e}\sin\Phi\tan\Theta & N_{\delta r}\cos\Phi\tan\Theta \end{bmatrix} \quad (26)$$

A well-defined vector relative degree [15] exists if and only if $A(\bar{x})$ is non-singular. Its determinant is given by

$$\det A(\bar{x}) = X_{\delta P}L_{\delta a}M_{\delta e}N_{\delta r}\{\cos(\Psi-\lambda_A)\cos\lambda_E+\sin\lambda_E\tan\Theta\} \quad (27)$$

Since we regulate range, bank angle and the bearing rates, the system has a well-defined vector relative degree $\{2,1,1,2\}$ unless the quantity in braces is zero.

The process of dynamic inversion ignores the nonlinearities and leader's acceleration terms in Eq.(24). Thus, an approximate feedback linearization is given as follows:

$$\begin{bmatrix} \delta T \\ \delta a \\ \delta e \\ \delta r \end{bmatrix} = \begin{bmatrix} \\ A(\bar{x}) \\ \\ \end{bmatrix}^{-1} \begin{bmatrix} \nu_R \\ \nu_{\dot{\chi}_A} \\ \nu_{\dot{\chi}_E} \\ \nu_\Phi \end{bmatrix} \quad (28)$$

where the vector $\bar{\nu} = \begin{bmatrix} \nu_R & \nu_{\dot{\chi}_A} & \nu_{\dot{\chi}_E} & \nu_\Phi \end{bmatrix}^T$ represents the *pseudo-control* input vector and represents the desired dynamics of the output vector $\begin{bmatrix} R, & \dot{\lambda}_A-\dot{\Psi}, & \dot{\lambda}_E-\dot{\Theta}, & \Phi \end{bmatrix}^T$. Thus, the system dynamics, as far as the regulated output variables are concerned, from Eq. (25) and (28), is given by

$$\bar{y}^{(r)} = \bar{\Delta} + \bar{\nu}$$

where $\bar{y}^{(r)} = \begin{bmatrix} \ddot{R} & \ddot{\lambda}_A-\ddot{\Psi} & \ddot{\lambda}_E-\ddot{\Theta} & \ddot{\Phi} \end{bmatrix}^T$, where $r=\{2,1,1,2\}$ is the vector relative degree and $\bar{\Delta} = \bar{\Delta}(\bar{x}, \bar{a}_L, t)$ is the modeling error vector consisting of the LOS variables, leader acceleration terms and follower aircraft motion variables.

The bank angle command is constructed to maintain turn coordination, that is, to nullify the side acceleration along the Y-axis of the body fixed frame. This can be accomplished in several ways. One such way is to use a PD controller to regulate the side acceleration to zero as in Fig. 3.

2. Controller Design using Adaptive Output Feedback

The objective of the control design is for the output vector $\bar{y} = \begin{bmatrix} R & \dot{\lambda}_A-\dot{\Psi} & \dot{\lambda}_E-\dot{\Theta} & \Phi \end{bmatrix}^T$ to track a stable, bounded reference trajectory vector $\bar{y}_c$. The *pseudo-control* is chosen to have the form [13,14]

$$\bar{\nu} = \bar{y}_c^{(r)} + \bar{\nu}_{dc} - \bar{\nu}_{ad} \quad (29)$$

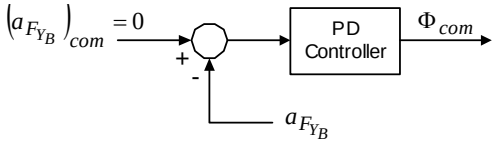

Figure 3. Bank angle command for Turn Coordination

where $\bar{y}_c^{(r)}$, the r^{th} derivatives of the reference trajectory vector $\bar{y}_c$, are generated by stable reference models that define the desired closed-loop behavior, $\bar{\nu}_{dc}$ is the vector output of linear dynamic compensators designed to stabilize the linearized error dynamics, and $\bar{\nu}_{ad}$ is the vector adaptive component designed to cancel the effect of the modeling error vector $\bar{\Delta}$.

Since range has relative degree 2, the plant transfer function from the *pseudo-control* ν_R to R is $1/s^2$. A first order lead-lag compensator structure was selected to stabilize the range error dynamics according to the direct adaptive output feedback approach of Ref. [13]. In addition, the pole-placement approach was used to satisfy the SPR condition. The resulting two outputs of the compensator are given by

$$\begin{bmatrix} \nu_{dc_R} \\ \tilde{y}_{ad_R} \end{bmatrix} = \frac{1}{s+7}\begin{bmatrix} 8(s+1) \\ 20(s+1) \end{bmatrix} \cdot \tilde{y}_R(s) \tag{30}$$

which places the closed-loop poles of the error dynamics at $-3, -1 \pm j$. The low pass filter $T_R^{-1}(s)$ was chosen as

$$T_R^{-1}(s) = \frac{1}{0.5s+1} \tag{31}$$

It is easy to verify that the transfer function $G_R(s)T_R(s)$ is SPR. A Sigma-Pi (SP) NN with 47 neurons and a bias term was used in the adaptive element. The aircraft motion variables $[U, V, W, p, q, r, \Phi, \Theta, \Psi]^T$, the LOS kinematics variables $[R, \lambda_A, \lambda_E]^T$, the current *pseudo-control* input ν_R, and the training signal from the compensator $\tilde{y}_{ad_R}$, were used in the input vector to the neurons. All the NN inputs were normalized using an estimate for their maximum values. The complete input vector consisted of these values together with a bias term. Thus, there are a total of 48 NN weights. The NN gains were set to F_R = 50 and λ_{w_R} = 1. Range was commanded to follow the output of a second order reference model, designed with a natural frequency of ω_{n_R} = 1 rad/sec and damping ς_R =0.8.

Since the bearing angle rates $\dot{\chi}_A$ and $\dot{\chi}_E$ are relative degree 1 outputs, the linear compensators corresponding to these outputs are just proportional error controllers. The gains of the proportional error controller were chosen as K_{χ_A} = 10 and K_{χ_E} = 10. Thus, their designs follow a state feedback approach, and the tracking error of the bearing angles rates are directly used as training signals for the NN. The command filter was chosen as a first order system with time constants of $\tau_{\chi_A} = \tau_{\chi_E}$ =1. The NN used in each channel has the same form as in the range channel except for the input vectors $\left[\nu_{\dot{\chi}_A}, \tilde{y}_{ad_{\dot{\chi}_A}}\right]^T$ and $\left[\nu_{\dot{\chi}_E}, \tilde{y}_{ad_{\dot{\chi}_E}}\right]^T$ and the network gains of F_{χ_A} = 100, $\lambda_{w_{\chi_A}}$ = 0.5 and F_{χ_E} = 100, $\lambda_{w_{\chi_E}}$ = 0.5.

The bank angle command Φ_{com} in Fig. 3 is filtered through a second order command filter to generate the reference bank angle command Φ_c. Since the bank angle has relative degree 2, a first order lead-lag compensator structure was selected to stabilize the bank angle error dynamics. By using pole-placement to satisfy the SPR condition, the resulting two outputs of the compensator are given by

$$\begin{bmatrix} \nu_{dc_\Phi} \\ \tilde{y}_{ad_\Phi} \end{bmatrix} = \frac{1}{s+10}\begin{bmatrix} 8(s+1) \\ 20(s+1) \end{bmatrix} \cdot \tilde{y}_\Phi(s) \tag{32}$$

which places the closed-loop poles of the error dynamics at $-3, -1 \pm j$. The low pass filter $T_\Phi^{-1}(s)$ was chosen as

$$T_{\Phi}^{-1}(s) = \frac{1}{0.5s+1} \tag{33}$$

so that the transfer function $G_{\Phi}(s)T_{\Phi}(s)$ is SPR. A Sigma-Pi (SP) NN with 47 neurons and a bias term was used in the adaptive element. The variables $\left[U, V, W, P, Q, R, \Phi, \Theta, \Psi, R, \lambda_A, \lambda_E, \nu_{\Phi}, \tilde{y}_{ad_{\Phi}}\right]^T$ were used as inputs to the NN. All of the NN inputs were normalized using an estimate for their maximum values. The complete input vector consisted of these values together with a bias term. Thus, there are a total of 48 NN weights. The network gains were F_{Φ} = 100 and $\lambda_{w_{\Phi}}$ = 1. The bank angle was commanded to follow the output of a second order reference model, designed with a natural frequency of $\omega_{n_{\Phi}}$ = 5 rad/sec and damping ς_{Φ} =0.8.

The NN adaptation rule for each channel is given from the extensions of Lyapunov theory [20]

$$\dot{\hat{W}} = -F\left(\tilde{y}_{ad}\phi_f + \lambda_w \hat{W}\right) \tag{34}$$

where $F > 0$ and $\lambda_W > 0$ are the adaptation gains and ϕ_f is the basis function vector ϕ after being filtered through $T^{-1}(s)$. Fig. 4 shows a block diagram implementation of the controller design.

3. Pseudo-Control Hedging (PCH)

Any dynamics and nonlinearities associated with actuators have not yet been considered in the design. If the actuators become position or rate saturated, the reference models will continue to demand tracking as though full authority were still available. Furthermore, when an adaptive element such as a neural network is introduced, these actuator nonlinearities will appear in the tracking error dynamics resulting in the adaptive element attempting to correct for them. PCH is introduced to protect the adaptive law from effects due to actuator rate and position limits, unmodeled actuator dynamics and to protect the adaptive process when it is not in control of the plant. The main idea behind PCH methodology is to modify the reference command in order to prevent the adaptive element from adapting to these actuator characteristics, while allowing adaptation to other effects to continue. This is commonly done by generating the command using a reference model for the desired response. The reference model is 'hedged' by an amount equal to the difference between the commanded and an estimate for the achieved *pseudo-control* [19].

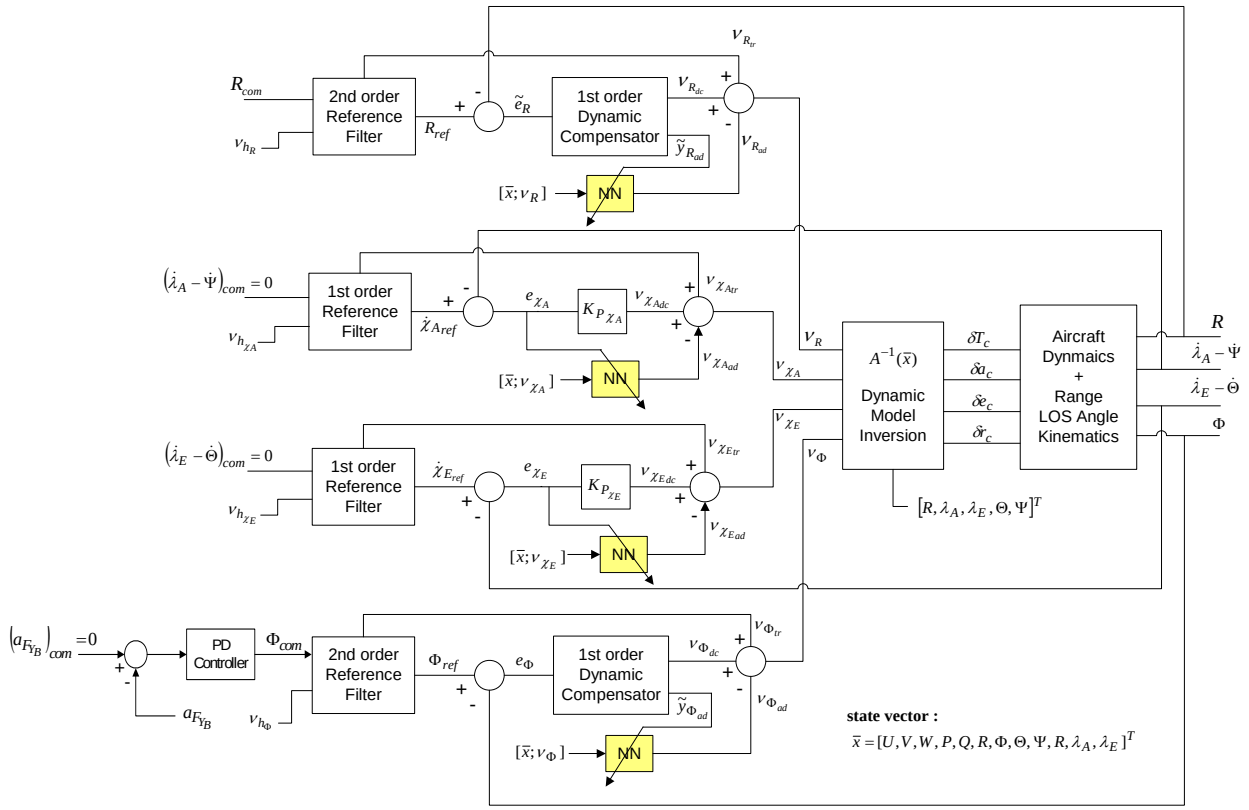

Figure 4. Integrated Guidance and Control Logic Block Diagram for Follower Aircraft – Design 1

4. Remark

The IGC design developed above leads to unacceptably large sideslip angles as will be shown in the simulation results. The problem here can be noticed by examining the first three rows of Eq. (25) and the matrix $A(\bar{x})$ in Eq. (26). It can be seen that the derivatives $\ddot{R}$, $\ddot{\lambda}_A - \ddot{\Psi}$ and $\ddot{\lambda}_E - \ddot{\Theta}$ do not contain the aileron deflection term δ_a. Specifically, the term $\ddot{\lambda}_A - \ddot{\Psi}$, which is the second derivative of the azimuth bearing angle $\lambda_A - \Psi$, shows strong dependence on the rudder deflection δ_r for small bank angle Φ. This implies that the rudder is used to generate a heading rate to regulate the azimuth bearing rate to zero. Using the rudder in this way causes uncoordinated turns leading to unacceptably large sideslip angles. In the next section, the azimuth channel is redesigned using the approach of adaptive backstepping [9,10] to avoid using the rudder to control the azimuth rate.

IV. Integrated Guidance and Control using Neural Networks – Design 2

The idea behind the redesign of the azimuth channel is to show that there exists a natural dependency of the azimuth rate derivative $\ddot{\lambda}_A$ on the bank angle Φ, and consequently on the aileron deflection δa. Then this natural dependency can be exploited in a strategy to implement adaptive backstepping in terms of three feedback loops as follows

$$(\dot{\lambda}_A) \rightarrow (\phi) \rightarrow (p) \rightarrow (\delta a)$$

A. Azimuth rate control via backstepping design

The first step is to re-write Eq. (14) as follows

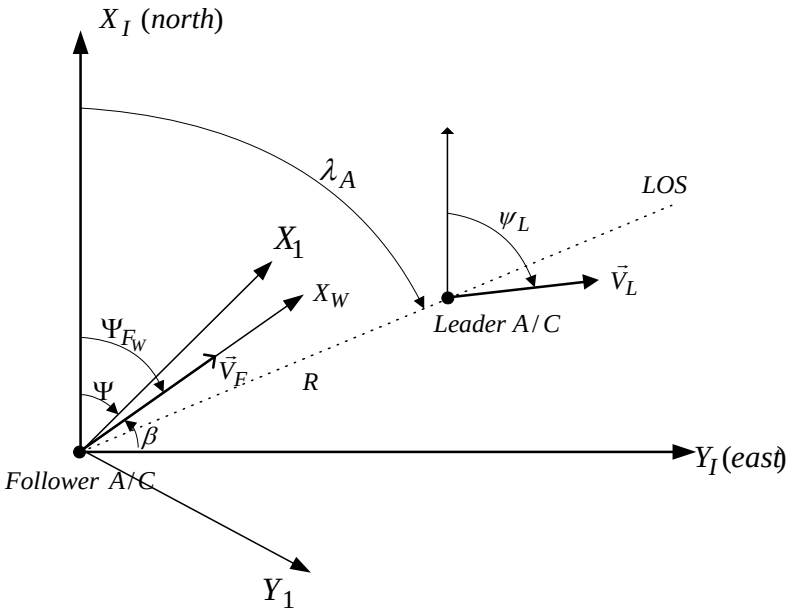

Figure 5. Coordinate Reference Frames in Horizontal Plane

$$\ddot{\lambda}_A = \frac{-2\dot{\lambda}_A}{\cos\lambda_E}\left[\left(\frac{\dot{R}}{R}\right)\cos\lambda_E - \dot{\lambda}_E \sin\lambda_E\right] + \left(\frac{1}{R\cos\lambda_E}\right)\left[-a_{L_{X_I}}\sin\lambda_A + a_{L_{Y_I}}\cos\lambda_A - \left(-a_{F_{X_I}}\sin\lambda_A + a_{F_{Y_I}}\cos\lambda_A\right)\right] \tag{35}$$

where $a_{F_{X_I}}$ and $a_{F_{Y_I}}$ represent the X and Y-axis acceleration components of follower aircraft expressed in the Cartesian inertial coordinates, respectively. Then the following equality can be derived

$$-a_{F_{X_I}}\sin\lambda_A + a_{F_{Y_I}}\cos\lambda_A = -a_{F_{X_1}}\sin(\lambda_A - \Psi) + a_{F_{Y_1}}\cos(\lambda_A - \Psi) \tag{36}$$

where $a_{F_{X_1}}$ and $a_{F_{Y_1}}$ represent the X and Y-axis acceleration components of follower aircraft expressed in the coordinate frame obtained by a rotation about the inertial Z-axis by the Euler angle Ψ. From the pictorial representation of the coordinate frames in the inertial horizontal plane, the acceleration component $a_{F_{Y_1}}$ can be approximated as follows

$$a_{F_{Y_1}} \approx V_F\cos\Theta\cdot\dot{\Psi}_{F_W} \approx V_F\cos\Theta\left(\dot{\Psi} + \dot{\beta}\right) \tag{37}$$

where the subscript '*W*' indicates the wind axes. Then, the following identities can be used to expand Eq. (37)

$$\dot{\Psi} = (q\sin\Phi + r\cos\Phi)\sec\Theta \tag{38}$$

$$\dot{\beta} = p\sin\alpha - r\cos\alpha + \frac{1}{mV_F}(D\sin\beta + Y\cos\beta) + \frac{g}{V_F}(\cos\alpha\sin\beta\sin\Theta + \cos\beta\sin\Phi\cos\theta - \sin\alpha\sin\beta\cos\Phi\cos\Theta) \tag{39}$$

Eq. (35) can be re-written as follows by utilizing Eq. (36)-(39)

$$\ddot{\lambda}_A = f_1(\bar{x}) + g_1(\bar{x}) \cdot \Phi + \Delta_{\lambda_A}(\bar{x}, \bar{a}_L) \tag{40}$$

where

$$\begin{aligned} f_1(\bar{x}) &= \frac{-2\dot{\lambda}_A}{\cos\lambda_E}\left[\left(\frac{\dot{R}}{R}\right)\cos\lambda_E - \dot{\lambda}_E \sin\lambda_E\right] - \left(\frac{1}{R\cos\lambda_E}\right) a_{F_{X_1}} \sin(\lambda_A - \Psi) \\ g_1(\bar{x}) &= -\frac{\cos(\lambda_A - \Psi)}{R\cos\lambda_E}\left(V_F\, q + g\cos\beta\cos^2\Theta\right) \end{aligned} \tag{41}$$

are known, computable terms. We also have

$$\dot{\Phi} = f_2(\bar{x}) + g_2 p\,,\ f_2(\bar{x}) = (q\sin\Phi + r\cos\Phi)\tan\Theta\,,\ \ g_2 = 1 \tag{42}$$

$$\dot{p} = f_3(\bar{x}) + g_3\delta a + \Delta_p(\bar{x}, \delta a),\ f_3(\bar{x}) = L_v v + L_p p + L_r r\ ,\ g_3 = L_{\delta a} \tag{43}$$

where $f_2(\bar{x}), f_3(\bar{x}), g_2, g_3$ are known, computable terms. Eq.(40)-(43) show that the azimuth rate dynamics has a natural cascade form. That is, ϕ can be used as a virtual control for the $\dot{\lambda}_A$ dynamics, and p as a virtual control for the ϕ dynamics, with the control δa finally being computed to ensure $\dot{\lambda}_A$ command tracking. Let $x_1 \equiv \dot{\lambda}_A$, $x_2 \equiv \phi$, $x_3 \equiv p$, and $u \equiv \delta a$. Then Eq.(40)-(43) can be rewritten as follows:

$$\dot{x}_1 = f_1(\bar{x}) + g_1(\bar{x})x_2 + \Delta_{\lambda_A}(\bar{x}, \bar{a}_L) \tag{44}$$

$$\dot{x}_2 = f_2(\bar{x}, x_2) + x_3 \tag{45}$$

$$\dot{x}_3 = f_3(\bar{x}, x_3) + g_3 u + \Delta_p(\bar{x}, \delta a) \tag{46}$$

where Δ_{λ_A} and Δ_p are modeling error terms and are functions of the states of the system $\bar{x}$ shown in Eq. (16), the leader acceleration terms $\bar{a}_L$, and the control deflection δa.

With the plant dynamics cast in the proper form, an adaptive backstepping method is presented. We begin by defining the following error states

$$\zeta_1 \equiv x_{1_c} - x_1 \tag{47}$$

$$\zeta_2 \equiv g_1 \cdot (\bar{x}_2 - x_2) \tag{48}$$

$$\zeta_3 \equiv g_1 \cdot (\bar{x}_3 - x_3) \tag{49}$$

where $\bar{x}_2$ and $\bar{x}_3$ are virtual commands to be constructed that will ensure that the command x_{1_c} is tracked.

Step 1: Differentiating ζ_1 of Eq.(47) and applying Eq. (44) and (48) yields

$$\dot{\zeta}_1 = \dot{x}_{1_c} - \dot{x}_1 = \dot{x}_{1_c} - f_1 - g_1 x_2 - \Delta_1 = \dot{x}_{1_c} - f_1 + \zeta_2 - g_1\bar{x}_2 - \Delta_{\lambda_A} \tag{50}$$

where $\bar{x}_2$ is viewed as a virtual control for the ζ_1 dynamics. Then to stabilize Eq. (50), let

$$\bar{x}_2 = g_1^{-1}\left[K_1\zeta_1 - f_1 + \dot{x}_{1_c} - \nu_{ad_1}\right] \tag{51}$$

where ν_{ad_1} is an adaptive control term designed to cancel Δ_{λ_A}. Then substituting Eq.(51) into Eq.(50) yields

$$\dot{\zeta}_1 = -K_1\zeta_1 + \zeta_2 + \nu_{ad_1} - \Delta_1 \tag{52}$$

where $\Delta_1 = \Delta_{\lambda_A}$. In ideal conditions, $\nu_{ad_1} = \Delta_1$ and $x_2 \to \bar{x}_2$, so the error $\zeta_2 \to 0$, and the ζ_1 dynamics become asymptotically stable.

Step 2: Differentiating ζ_2 yields

$$\begin{aligned}\dot{\zeta}_2 &= \dot{g}_1(\bar{x}_2 - x_2) + g_1\left(\dot{\bar{x}}_2 - \dot{x}_2\right) = \dot{g}_1(\bar{x}_2 - x_2) + g_1\dot{\bar{x}}_2 - g_1\dot{x}_2 \\ &= -\Delta_2 + \ddot{x}_{1_c} - g_1x_3 - g_1f_2 = -\Delta_2 + \ddot{x}_{1_c} - g_1f_2 + \zeta_3 - g_1\bar{x}_3\end{aligned} \tag{53}$$

where $\Delta_2 \equiv -\left[\dot{g}_1(\bar{x}_2 - x_2) + g_1\dot{\bar{x}}_2 - \ddot{x}_{1_c}\right]$ since the derivatives of f_1 and g_1 contain unknown terms due to leader aircraft motion. Let

$$\bar{x}_3 = g_1^{-1}\left[\zeta_1 + K_2\zeta_2 + \ddot{x}_{1_c} - g_1f_2 - \nu_{ad_2}\right] \tag{54}$$

so that

$$\dot{\zeta}_2 = -\zeta_1 - K_2\zeta_2 + \zeta_3 + \nu_{ad_2} - \Delta_2 \tag{55}$$

The purpose of introducing ζ_1 in Eq.(55) is to compensate for the coupling between the ζ_1 and ζ_2 dynamics. The sign of the ζ_1 in Eq.(54) is intentionally chosen as negative to set up a skew-symmetric matrix representing the complete error dynamics. This skew-symmetric structure is a key feature of backstepping controllers, and results in the cancellation of the coupling terms during Lyapunov stability analysis [10].

Step 3: This last step is very similar to the previous ones except that rather than the virtual control, the actual control signal is constructed. Differentiating ζ_3 yields

$$\begin{aligned}\dot{\zeta}_3 &= \dot{g}_1(\bar{x}_3 - x_3) + g_1\left(\dot{\bar{x}}_3 - \dot{x}_3\right) = \dot{g}_1(\bar{x}_3 - x_3) + g_1\dot{\bar{x}}_3 - g_1\dot{x}_3 \\ &= \dot{g}_1(\bar{x}_3 - x_3) + g_1\dot{\bar{x}}_3 - g_1\left(f_3 + g_3u + \Delta_P\right) = -\Delta_3 + \ddot{x}_{1_c} - g_1f_3 - g_1g_3u\end{aligned} \tag{56}$$

where $\Delta_3 \equiv -\left[\dot{g}_1(\bar{x}_3 - x_3) + g_1\dot{\bar{x}}_3 - \ddot{x}_{1_c} - g_1\Delta_p\right]$. Let

$$u = (g_1g_3)^{-1}\left[\zeta_2 + K_3\zeta_3 - g_1f_3 + \ddot{x}_{1_c} - \nu_{ad_3}\right] \tag{57}$$

so that

$$\dot{\zeta}_3 = -\zeta_2 - K_3\zeta_3 + \nu_{ad_3} - \Delta_3 \tag{58}$$

In this application, the absolute value of bearing angle, $|\psi_F - \lambda_A|$ should be kept less than $\frac{\pi}{2}$. The control power $g_3 = L_{\delta a}$ remains non-zero in most aircraft control applications. Eq.(52), (55), and (58) can be now expressed in state space form

$$\dot{z} = \bar{A}z + \nu_{ad} - \Delta \tag{59}$$

where $z \equiv [\zeta_1, \zeta_2, \zeta_3]^T$, $\nu_{ad} \equiv [\nu_{ad_1}, \nu_{ad_2}, \nu_{ad_3}]^T$, $\Delta \equiv [\Delta_1, \Delta_2, \Delta_3]^T$, and

$$\bar{A} = \begin{bmatrix} -K_1 & 1 & 0 \\ -1 & -K_2 & 1 \\ 0 & -1 & -K_3 \end{bmatrix} \tag{60}$$

The gains $K_{1,2,3} > 0$ to ensure stability, but they also need to be tuned to obtain reasonable performance. The complete control policy is given by Eq.(51), (54), and (57). The block diagram for this control structure is given by Fig. 2. The detailed proof of stability of closed-loop system and the derivation of the adaptation law are referred to Ref. [9] and the references within.

B. Turn Coordination – Adaptive side acceleration control

To maintain turn coordination, the side acceleration along the y-axis of the body-fixed frame a_{Y_B} is regulated to zero. The control design consists of an outer-loop proportional-integral (PI) controller acting on the side acceleration command error and whose output z_{com} is a command for the blended output $z = \beta + C_r r$ [22]. The signal z_{com} is input to an inner-loop inverting controller augmented by an adaptive NN that generates rudder deflection command δr_{com}. The details of the design are contained in Ref. [22].

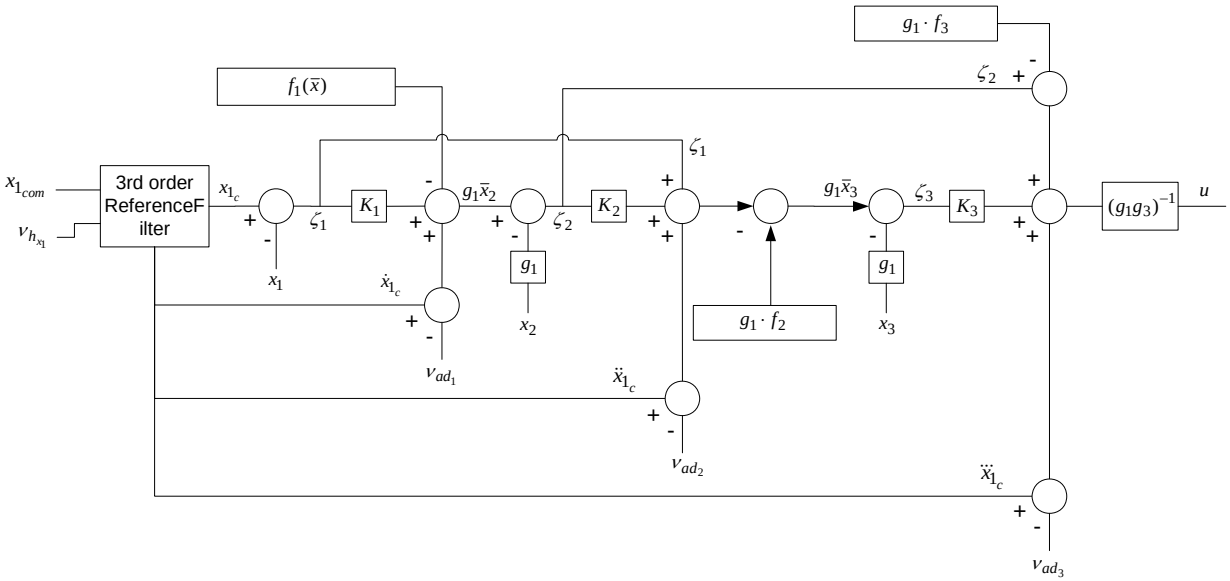

Figure 6. Control Structure of LOS Azimuth Angle Channel using Adaptive Backstepping Algorithm

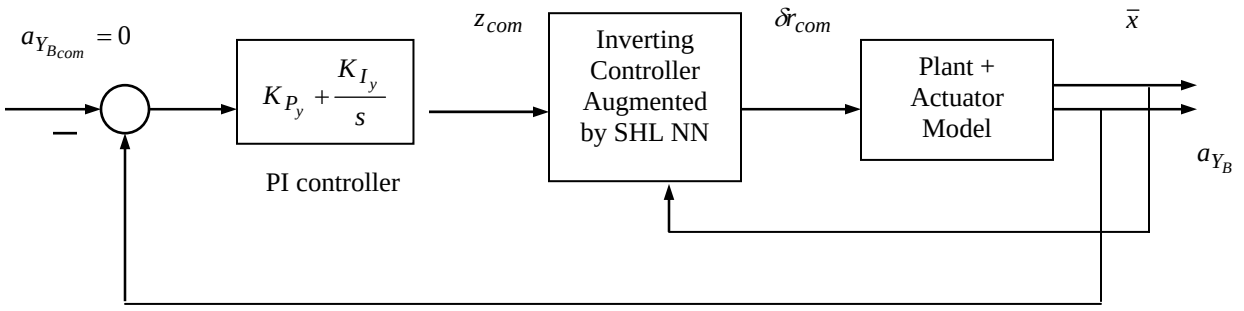

Figure 7. Side acceleration controller

C. Dynamic Inversion

From the modified design for azimuth rate control and turn coordination above, the equation for dynamic inversion to determine the actuator deflection commands can be set up as follow

$$\begin{bmatrix} \ddot{R} \\ \dot{\zeta}_3 \\ \ddot{\lambda}_E - \ddot{\Theta} \\ \dot{z} \end{bmatrix} = \begin{bmatrix} \bar{\Delta}_2(\bar{x}, \bar{a}_L, t) \end{bmatrix} + \begin{bmatrix} A_2(\bar{x}) \end{bmatrix} \begin{bmatrix} \delta T \\ \delta a \\ \delta e \\ \delta r \end{bmatrix} \tag{61}$$

where

$$A_2(\bar{x}) = \begin{bmatrix} -X_{\delta T}\{\cos(\Psi - \lambda_A)\cos\lambda_E \cos\Theta + \sin\lambda_E \sin\Theta\} & 0 & 0 & 0 \\ 0 & g_1(\bar{x})g_3 & 0 & 0 \\ X_{\delta T}\{\cos(\Psi - \lambda_A)\sin\lambda_E \cos\Theta - \cos\lambda_E \sin\Theta\}/R & 0 & -M_{\delta e}\cos\Phi & N_{\delta r}\sin\Phi \\ 0 & 0 & 0 & \frac{Y_{\delta r}}{U_0} + C_r N_{\delta r} \end{bmatrix} \tag{62}$$

where U_0 is the trim speed of the aircraft, the value for C_r can be obtained by following the design procedure in Ref.[22], and $\bar{\Delta}_2(\bar{x}, \bar{a}_L, t)$ is the modeling error vector different from the one in Eq. (25). Thus, an approximate feedback linearization is given as follows:

$$\begin{bmatrix} \delta T \\ \delta a \\ \delta e \\ \delta r \end{bmatrix} = \begin{bmatrix} A_2(\bar{x}) \end{bmatrix}^{-1} \begin{bmatrix} \nu_R \\ \nu_{\zeta_3} \\ \nu_{\dot{\lambda}_E} \\ \nu_z \end{bmatrix} \tag{63}$$

where the vector $\bar{\nu} = \begin{bmatrix} \nu_R & \nu_{\zeta_3} & \nu_{\dot{\lambda}_E} & \nu_z \end{bmatrix}^T$ represents the *pseudo-control* input vector and represents the desired dynamics of the vector $\begin{bmatrix} R, & \zeta_3, & \dot{\lambda}_E - \dot{\Theta}, & z \end{bmatrix}^T$. The rest of the control design is very similar to the design presented in Section III B.2, the details of which can be found in Refs.[13] and [14]. The block diagram of the overall system is shown in Fig. 8.

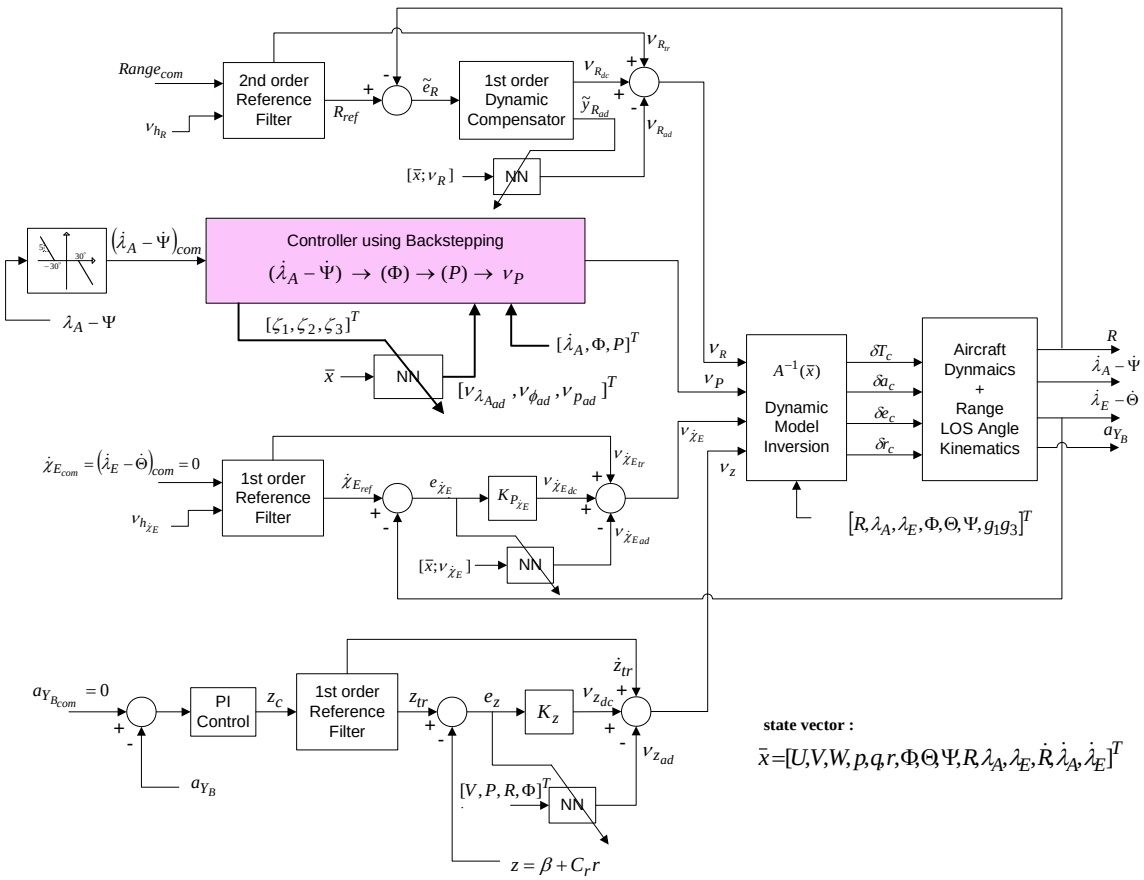

Figure 8. Integrated Guidance and Control Logic Block Diagram for Follower Aircraft – Design 2

V. Simulation-Based Evaluation

A. Time-Scale Separated Guidance and Control (TSSGC) Design

The TSSGC design is described in complete detail in Ref. [3]. This section just provides a summary. The TSSGC design consists of an outer-loop guidance block that takes as inputs range and LOS rate commands. With feedback of LOS variables and their derivatives, and the follower aircraft kinematics state information, the guidance block computes inertial acceleration commands by carrying out approximate dynamic inversion of the range and LOS rate kinematics. The inertial acceleration commands are transformed into normal $\left(a_{Z_B}\right)$ and longitudinal $\left(a_{X_B}\right)$ specific force commands, and a bank angle command. These commands along with a side acceleration command of zero are sent to an inner-loop autopilot. The autopilot consists of dynamic inversion based controllers for normal and side acceleration command tracking, and bank angle command tracking, plus a PI throttle controller for tracking a blend of the longitudinal acceleration and speed command V_{com}. NN based adaptation is introduced in the guidance block to compensate for modeling error due to unknown leader aircraft acceleration. NN based adaptation is also introduced in the autopilot to compensate for modeling error due to parametric aerodynamic modeling uncertainties.

B. Simulation Results

A nonlinear 6-DOF simulation with linearized aerodynamics is used for the testing of the control and guidance algorithms for formation flight. Quaternion attitude angles are obtained by integrating the rate gyros. The simulation model is a rigid body aircraft model with 13 states, 3 for position with respect to the Earth-fixed frame, 3 for translational velocity expressed in the body frame, 4 for the quaternions and 3 for the angular velocity expressed in

the body frame. Engine thrust is obtained from a linear interpolation map of throttle position. The actuators are modeled as first-order, stable linear filters with rate and position limits and time delays.

The IGC Design 1, IGC Design 2, and the TSSGC Design are evaluated on the basis of tracking a commanded range from a maneuvering leader aircraft. The commanded range is 5 meters, which is approximately two wing-span lengths of the follower aircraft. The LOS (bearing) rate commands for the TSSGC (IGC 1 and IGC 2) are nominally set to zero. In case the bearing angles drift to values greater than the field-of-view maximum widths, which are assumed to be $\pm 30^0$ for both the azimuth and elevation bearing angles, the LOS (bearing) rate commands are adjusted to keep the bearing angles within $\pm 30^0$.

The leader maneuver is a 3D slanted-box maneuver as shown in Fig. 9. The commanded speed of the leader aircraft is $V_{com} = 25$ meters/sec. The guidance and control design for the leader aircraft is the TSSGC design outlined in Section V-A above. The leader starts off at the origin $(0,0,0)$ and moves at constant velocity, then turns and climbs, turns again at constant altitude, and finally turns and descends to the starting point. All the results below include the effect of adaptation. In the absence of adaptation, the particular leader maneuver chosen results in closed-loop system instability of the follower aircraft with all the three guidance and control designs. This shows the vulnerability of the designs to modeling error due to leader accelerations and aerodynamic uncertainties.

Figures 10 a, b, and c show the range command tracking performance in meters with the TSSGC, IGC 1 and IGC 2 designs. The black solid line represents the commanded range $R_{com} = 5$ meters, the blue dotted line is the range, and the red dashed line represents the hedged reference signal. The range signal R tracks the hedged reference signal R_{ref}. It is clear that the performance with the IGC designs (Fig. 10 b, c) is superior to the TSSGC design (Fig. 10 a) by virtue of much smaller range overshoots (maximum of 1.5 meters for the IGC designs, versus 5 meters for the TSSGC design) from the commanded range, and convergence to the commanded range in steady-state. The overshoots in range occur after the leader aircraft starts a maneuver.

One of the reasons for the deficient performance of the TSSGC design when compared to the IGC design is the choice of command to the throttle controller in the TSSGC design. The throttle controller in the TSSGC design is a PI controller with anti-windup feature for commanding throttle position $\delta_{T_{com}}$. There is a stability issue when the longitudinal acceleration command $f_{x_{com}}$ from the guidance law is input to the throttle controller for the case of a sharply turning leader aircraft. This is due to the fact that the guidance logic generates an excessive negative acceleration command along the X-axis of the body frame (highly negative $f_{x_{com}}$) when starting a heading turn and this causes saturation into the lower bound of the throttle, ultimately leading to instability of the entire closed-loop system. The same reasoning is applicable to the leader aircraft. So for the leader aircraft, the command to the throttle controller consists of only the speed command V_{com}, and for the follower aircraft, the throttle controller command is modified to be a blend of the longitudinal acceleration command $f_{x_{com}}$ and speed command V_{com} as in Fig. 11, where $0 \le K_x \le 1$ is a design constant. This is arguably not a fair evaluation, since the follower aircraft cannot know a priori the commanded speed of the leader aircraft in a realistic setting. The throttle controller command in Fig. 11 reduces the transient speed of response of the range variable and the desired steady-state with respect to range is not exactly achieved (Fig. 10 a), even when the leader stops maneuvering. The gain K_x has to be chosen carefully and is obtained after several simulation runs for different leader maneuvers, to get acceptable range tracking performance while not saturating the throttle controller. The consequence of the modification of the throttle command is the trade-off between range command tracking and closed-loop stability for the TSSGC design. This is not an issue in the IGC designs since the throttle command is obtained by the dynamic inversion of the range and bearing rates' dynamics (Eq. 28 and Eq. 63) with adaptive compensation for the modeling errors.

Figures 12 a, b, and c show the LOS and bearing rates histories in degrees per second with the TSSGC and IGC designs. When the leader maneuvers, there are large overshoots in the LOS and bearing rates histories, but the overshoots with the IGC designs are much smaller than those with the TSSGC design.

Figures 13 a, b, and c show the actuator deflections with the TSSGC, IGC 1 and IGC 2 designs. With the IGC designs, there is lot more activity in the rudder and aileron channels with the IGC designs than with the TSSGC design.

Figures 14 a, b, and c show the angle of attack and sideslip angle histories in degrees with the TSSGC, IGC 1 and IGC 2 designs. It is clear that the sideslip angles with IGC design 1 are unacceptably large (maximum 15 degrees). With the TSSGC design and IGC design 2, the sideslip angle histories are acceptable (maximum 4 degrees).

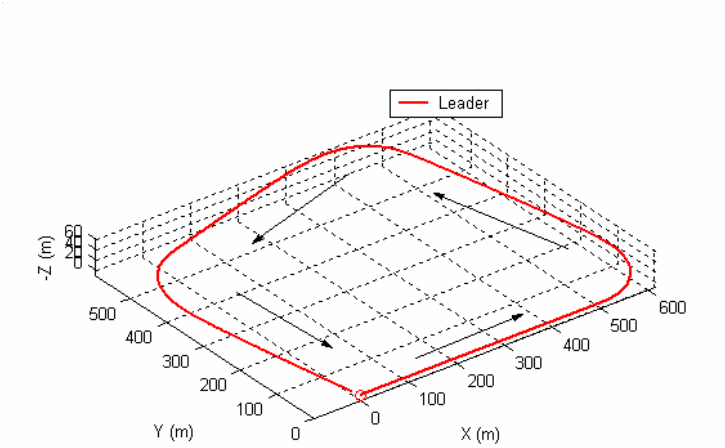

Figure 9. Leader 3D slanted-box Trajectory (meters)

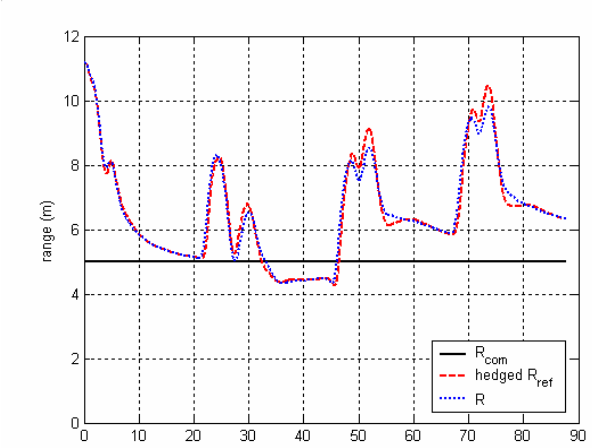

10 a

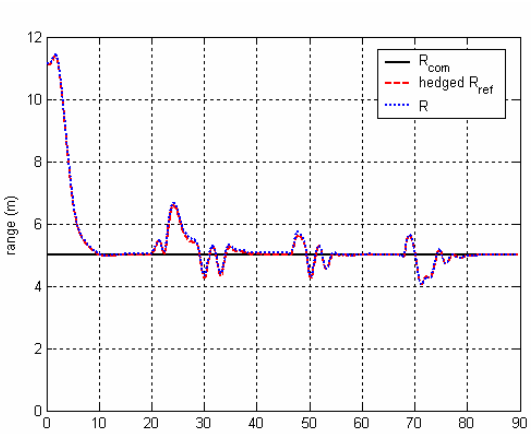

10 b

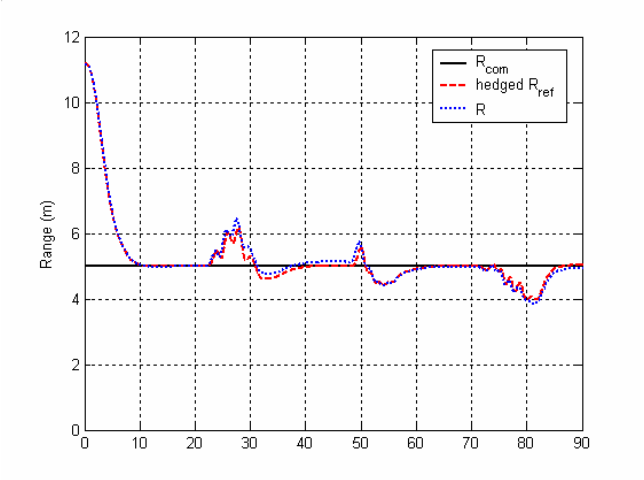

10 c

Figure 10. Range Command Tracking (meters), a) TSSGC Design, b) IGC Design 1, c) IGC Design 2

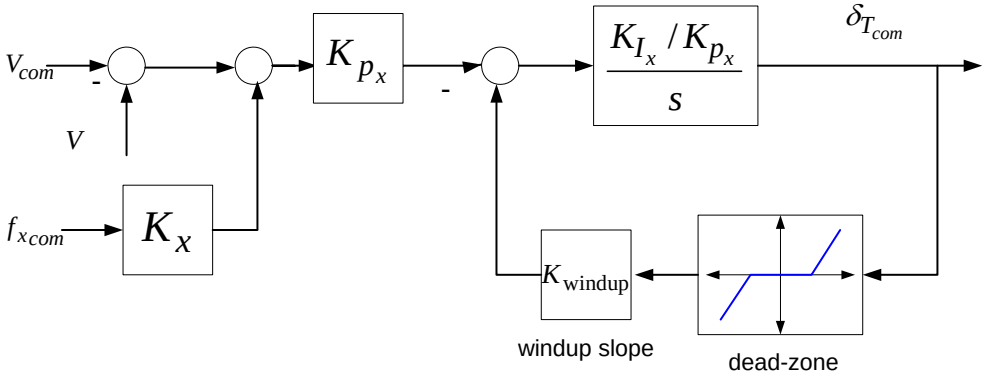

Figure 11. Throttle Controller in TSSGC design

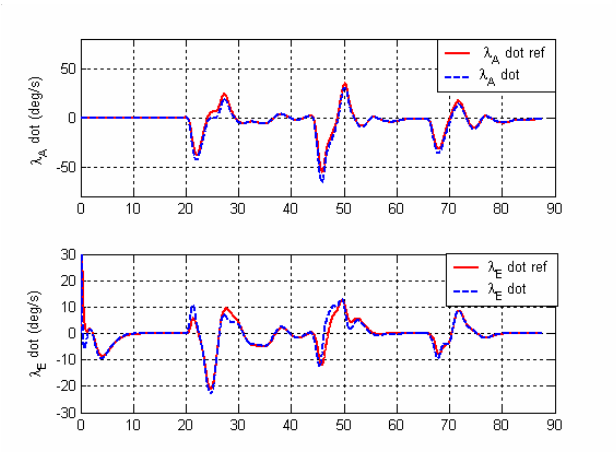

12 a

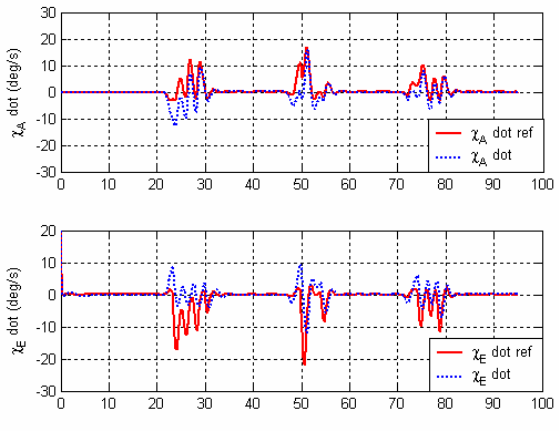

12 b

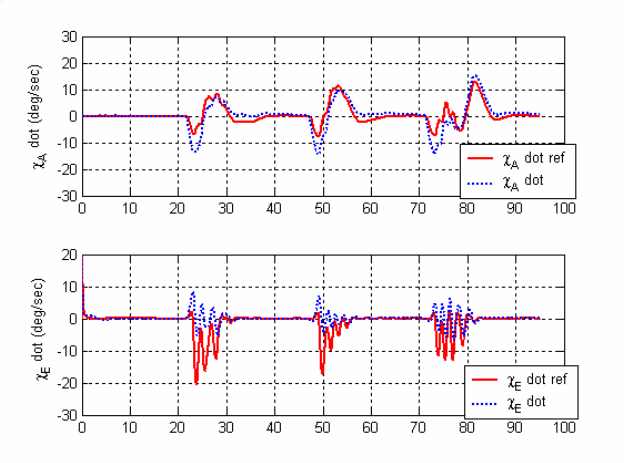

12 c

Figure 12. LOS and Bearing rates Tracking (deg/s), a) TSSGC Design, b) IGC Design 1, c) IGC Design 2

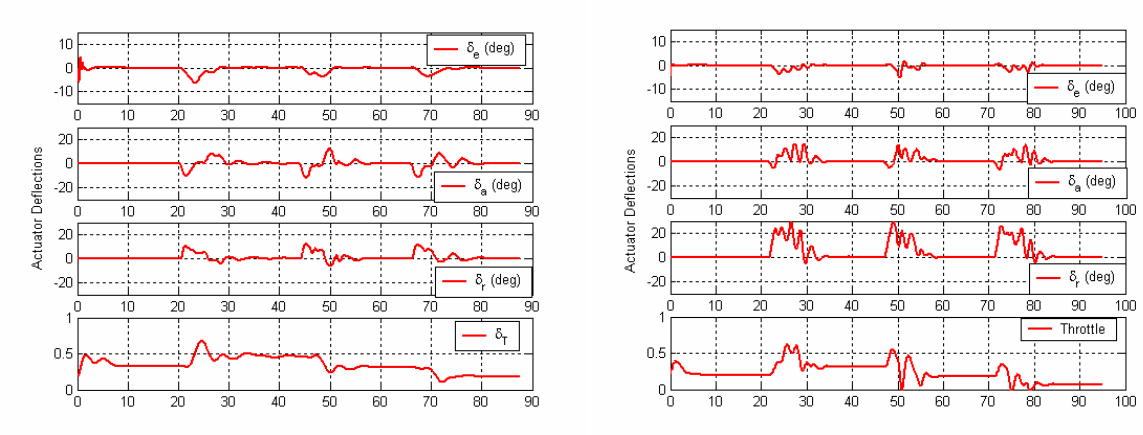

13 a **13 b**

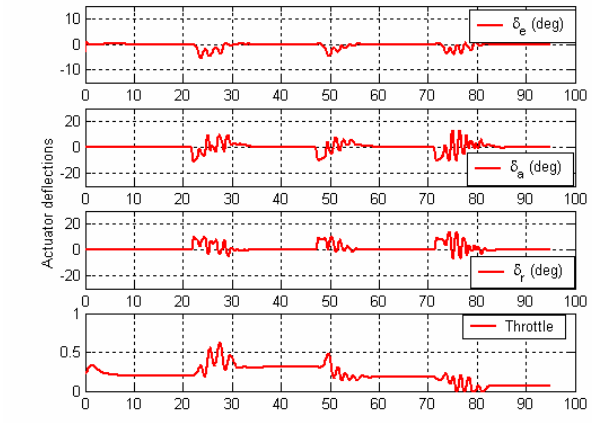

13 c

Figure 13. Actuator deflection histories a) TSSGC Design, b) IGC Design 1, c) IGC Design 2

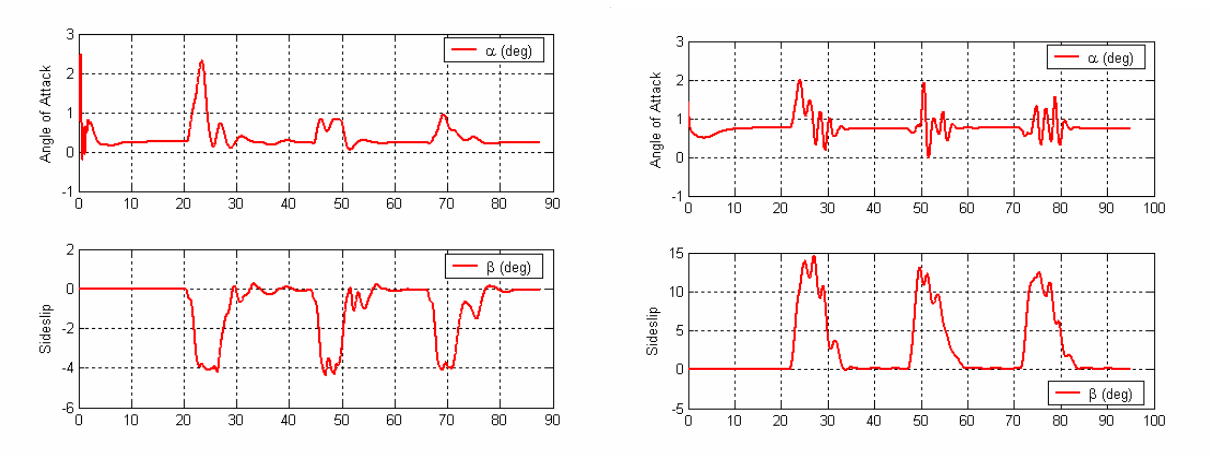

14 a **14 b**

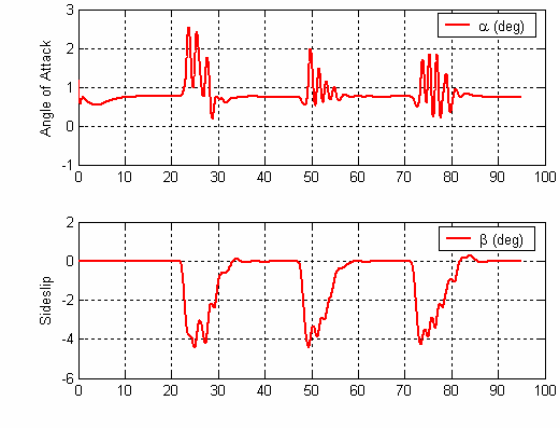

14 c

Figure 14. Aerodynamic Angles (deg) a) TSSGC Design, b) IGC Design 1, c) IGC Design 2

VI. Conclusions

This paper has presented an IGC design for formation flight using a combination of adaptive output feedback and backstepping techniques without an underlying time-scale separation assumption. The design objective was to regulate the range and two bearing angle rates with respect to a maneuvering leader aircraft and maintaining turn coordination. Neural network based online adaptation is used to compensate for modeling errors in the design process, that include, uncertainties due to unknown leader aircraft acceleration, and the modeling error due to parametric uncertainties in the aircraft aerodynamic derivatives. We have drawn a couple of conclusions from our design process and simulation results. The first conclusion is that adaptation is critical to the stability of the IGC design. Secondly, when compared to an adaptive TSSGC design, the adaptive IGC design offers an explicit advantage of using higher gains in the design. In the case of the time-scale separated design, using large gains in the guidance block can lead to large commands to the autopilot, increasing the potential for actuator saturation and eventual instability. This advantage of the IGC design translates into better transient and steady-state range tracking performance as seen in the simulation results.

Future research involves integrating the IGC design with a target-tracking estimation design and image processing followed by flight test evaluations of the complete design in vision-based formation flight of a maneuvering leader and follower aircraft.

Acknowledgments

This research has been sponsored under AFOSR contract F4960-01-1-0024 and under NRTC contract NCC 2-945.

References

[1] A. Betser, P. Vela, and A. Tannenbaum, "Automatic Tracking of Flying Vehicles Using Geodesic snakes and Kalman filtering," *IEEE Conference on Decision and Control*, Vol. 2, pp 1649-1654, December 2004.

[2] L. Polloni, R. Mati, M. Innocenti, G. Campa and M. Napolitano, "A Synthetic Environment for the Simulation of Vision-based Formation Flight, " *AIAA Modeling and Simulation Technologies Conference*, Austin, Texas, August 2003.

[3] R. Sattigeri, A. J. Calise, B.S. Kim, K. Volyanskyy and N. Kim, "6 DOF Nonlinear Simulation of Vision-based Formation Flight," *AIAA Guidance, Navigation, and Control Conference*, San Francisco, CA, August 2005.

[4] P. K. Menon and E..J. Ohlmeyer, "Integrated Design of Agile Missile Guidance and Autopilot Systems," *IFAC – Control Engineering Practice*, Vol. 9, pp. 1095-1106, 2001.

[5] P. K. Menon, G. D. Sweriduk and E..J. Ohlmeyer, "Optimal Fixed-Interval Integrated Guidance-Control Laws for Hit-to-Kill Missiles," *AIAA Guidance, Navigation, and Control Conference*, Austin, TX, August 2003.

[6] I. Shkolnikov, Y. Shtessel, and D. Lianos, "Integrated Guidance-Control System of a Homing Interceptor - Sliding Mode Approach," *AIAA Guidance, Navigation, and Control Conference*, Montreal, Canada, August 2001.

[7] C.F. Lin, Q. Wang, J.H. Speyer, J.H. Evers, and J.H. Cloutier, "Integrated Estimation, Guidance and Control System Design using Game Theoretic Approach," *American Control Conference*, pp 3220-3224, 1992.

[8] N.F. Palumbo and T.D. Jackson, "Integrated Missile Guidance and Control: A State Dependent Riccati Differential Equation Approach," *IEEE International Conference on Control Applications*, Vol. 1, pp. 243-248, August 1999.

[9] M. Sharma and N. Richards, "Adaptive, Integrated Guidance and Control for Missile Interceptors," *AIAA Guidance, Navigation, and Control Conference*, Providence, RI, August 2004.

[10] M. Krstic, I. Kanellakopoulos and P. Kokotovic, *Nonlinear and Adaptive Control Design*, John Wiley & Sons, Inc., New York, 1995.

[11] E. Johnson and S. Kannan, "Adaptive Flight Control for an Autonomous Unmanned Helicopter," *AIAA Guidance, Navigation, and Control Conference*, Monterey, CA, August 2002.

[12] E. Johnson, and A.J. Calise, "Feedback Linearization with Neural Network Augmentation applied to X-33 Attitude Control," *AIAA-2000-4157 Guidance, Navigation and Control Conference*, Denver, CO, August 2000.

[13] A.J. Calise, N. Hovakimyan and M. Idan, "Adaptive Output Feedback Control of Nonlinear Systems Using Neural Networks," *Automatica*, 2001, vol. 37, no. 8, pp 1201-1211.

[14] N. Hovakimyan, A.J. Calise and N. Kim, "Adaptive Output Feedback Control of a Class of Multi-Input Multi-Output Systems using Neural Networks," *International Journal of Control*, October 2004, vol. 77, no. 15, pp 1318-1329.

[15] A. Isidori, "*Nonlinear Control Systems*", Springer-Verlag, Berlin, 1989.

[16] J. Ha, C. Alvino, G. Pryor, M. Niethammer, E. Johnson, and A. Tannenbaum, "Active Contours and Optical Flow for Automatic Tracking of Flying Vehicles," *American Control Conference*, Vol. 4, pp 3441-3446, 2004.

[17] E. Johnson, A. Calise, R. Sattigeri, Y. Watanabe, and V. Madyastha, "Approaches to Vision-based Formation Control," *IEEE Conference on Decision and Control*, Vol. 2, pp 1643-1648, December 2004.

[18] V. Madyastha, and A.J. Calise, "An Adaptive Filtering Approach to Target Tracking," *American Control Conference*, pp. 1269-1274, June 2005.

[19] E. Johnson, and A.J. Calise, "Feedback Linearization with Neural Network Augmentation applied to X-33 Attitude Control," *AIAA-2000-4157 Guidance, Navigation and Control Conference*, Denver, CO, August 2000.

[20] K. Narendra and A. Annaswamy, "*Stable Adaptive Control*", Prentice Hall, Inc., 1995.

[21] B. Etkin, *Dynamics of Atmospheric Flight*, John Wiley & Sons, Inc., 1972.

[22] A.J. Calise, M. Sharma and E. J. Corban, "Adaptive Autopilot Design for Guided Munitions," *Journal of Guidance, Control and Dynamics*, Vol. 23, No. 5, Sept-Oct 2000.